Final Version, 2/23/98
Submitted To JGR

Airborne Passive Remote Sensing of the Troposphere in Nashville/Middle Tennessee Area During the 1995 Southern Oxidants Study

David M. Rider, Helen M. Worden, Reinhard Beer, Sumita Nandi
and Lawrence C. Sparks

Jet Propulsion Laboratory
California Institute of Technology
Pasadena, CA 91109

Abstract

In July of 1995 the Airborne Emission Spectrometer was deployed to Nashville, Tennessee to participate in the 1995 Ozone Study Intensive Campaign of the Southern Oxidants Study. AES is a high resolution mid-infrared interferometer that measures the spectrum of upwelling radiation in the 650-4250 cm^{-1} range. In Nashville the instrument was deployed on 6 flights each covering a ~80 x 100 km^2 area centered on downtown Nashville from an altitude of 6 km. The spectra obtained on these flights were inverted to provide maps of temperature, ozone, water vapor and carbon monoxide. This paper describes the collection, processing and analysis of the data, and compares the results with sonde and surface measurements. The results show that the spatial distribution of ozone and carbon monoxide are highly variable over the region, both in space and time. The highest levels of these two tropospheric pollutants were often observed at considerable distances from the urban center.

1. Introduction

The Southern Oxidants Study (SOS), initiated in 1988, is an ongoing investigation of the processes contributing to and controlling the formation of tropospheric ozone in the Southeastern United States. Its central goal is to understand why many areas of the Southeast consistently fail to meet the EPA's air quality standards, despite the fact that most of the region is only lightly industrialized. In the summer of 1995 a large number of field experiments, both ground and aircraft based, and investigators went to the Nashville

Tennessee area to participate in an intensive study of the chemistry, transport and meteorology of the region surrounding Nashville for the Southern Oxidant Study (SOS) Nashville/Middle Tennessee Ozone Study Intensive. *Meagher et al.* [1998] have given an overview of the ozone problem in the Southeast. Descriptions of the aircraft-based and ground-based investigations participating in 1995 campaign have been given by *Hübler et al.* [1998] and *Meagher et al* . [1998] respectively.

This paper describes the results obtained with the Airborne Emission Spectrometer (AES) during the SOS 1995 summer campaign. AES is a high-resolution (0.07 cm^{-1}) infrared spectrometer designed for remote sensing of the troposphere from an airborne platform. Between July 7 and July 15, 1995 AES made six four-hour flights in the vicinity of Nashville on the NASA/Wallops Flight Facility C130Q research aircraft. Described here are the results for flights on July 7, 11, 12 and 13 where the objective was to obtain detailed maps of the spatial distribution of atmospheric temperature, water vapor, ozone and carbon monoxide. The AES measurements are highly complementary to the *in situ* and lidar measurements made by five other aircraft based investigations participating in the study in that they provided contiguous spatial coverage over a relatively large area to arrive at a detailed picture of where ozone accumulated in the region during the sampled period.

Remote sensing with infrared spectrometry is a well established technique that has been applied to a broad range of remote sensing applications [*Beer*, 1992; *Persky*, 1995]. Of relevance is the Tropospheric Emission Spectrometer (TES) [*Beer and Glavich*, 1989; *Beer*, 1992], an instrument being developed for remote sensing of the troposphere. TES is also a high resolution interferometer that will map the composition of the troposphere from the Earth Observing System CHEM platform that is scheduled for launch in 2002. AES is a prototype instrument for TES that serves as a test bed for the development of the TES instrument and for TES data processing concepts.

2. Experiment

2.1 Instrumentation

AES is a high-resolution (0.07 cm^{-1}) infrared Fourier transform spectrometer that covers the spectral range 650 - 4250 cm^{-1} (2.35 - 15.4 μm) in 4 spectral channels chosen both to optimize the detector response and to limit the thermal background impinging on the detectors. The spectral bands observed by each channel are further constrained by

interchangeable filters, each roughly 250 cm^{-1} wide. Each channel has a 1 X 4 detector array of photovoltaic HgCdTe for the three shortest wavelength channels and of photoconductive HgCdTe for the longest wavelength channel. The detectors and filters are cooled to 65 K to minimize noise. Each detector pixel has an aspect ratio of 1:8 and views the ground with a solid angle of 1 x 8 $mrad^2$. During data processing the spectra from the four pixels within an array are averaged so that at 5.92 km above the surface, the altitude of the AES flights, the averaged spectra represent the view of a 24 x 48 m^2 spot on the ground.

The interferometer is a simple Michelson-type with the plane mirrors replaced by cube-corner reflectors. A DC motor driven lead screw drives one of the cube-corners over a path difference of ± 8.5 cm about zero path difference. Data are acquired in both directions, each interferogram occupying 2 seconds with 1 second for cube-corner carriage turn-around. The interferometer is held under a partial vacuum to reduce coupling of acoustic vibrations into the light path and to protect the KBr beamsplitter and compensator. A sketch of the optical layout is shown in Fig. 1. The instrument views the atmosphere in the nadir direction through a ZnSe window mounted in the underside of the plane that is large enough to permit observations of a given location on the ground for 20 - 30 seconds. Light entering through the window is intercepted by a two-axis gimbaled mirror whose rate of

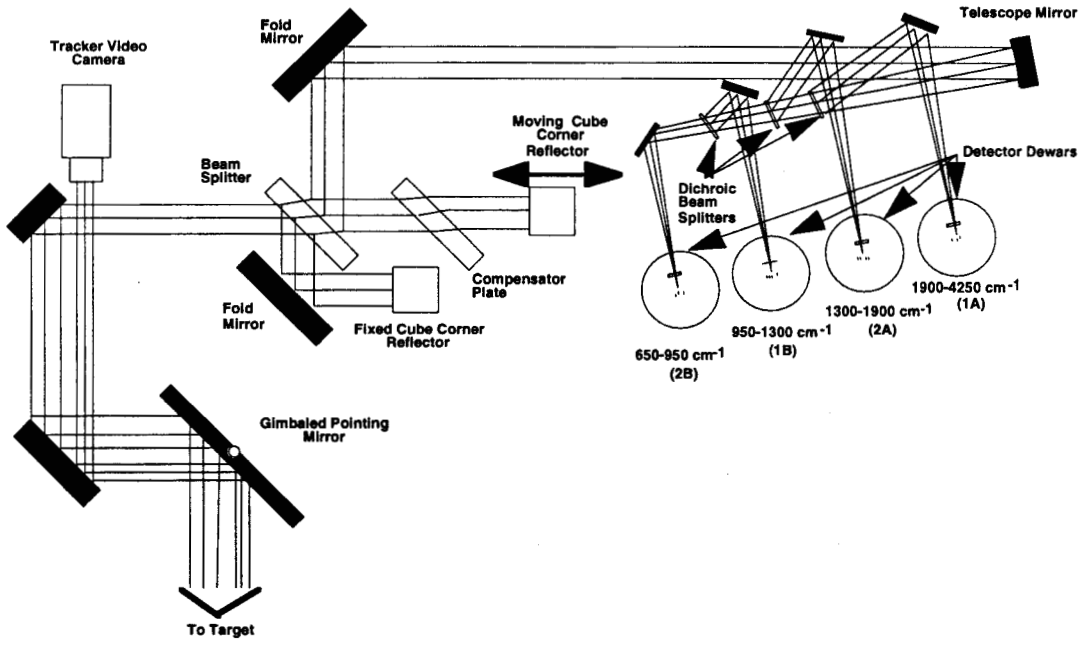

Figure 1. AES optical layout.

rotation can be set to provide image motion compensation which is essential for a Fourier transform spectrometer viewing inhomogeneous scenes. A joystick permits small manual corrections to the automatic rate compensation. A narrow-angle and a wide-angle TV camera, boresighted with the interferometer, provide the operator with a views of the scene on video monitors. Their outputs are recorded on video tape as a visible record of the observations. A radiometric blackbody target is also viewed by the gimbaled mirror for routine inflight radiometric calibrations. A periscope directs light from the gimbaled mirror into the interferometer. The interferometer and data collection are controlled by a ruggedized 486 PC. The location of the measurements are determined from GPS measurements of the plane's location.

2.2 Observation strategy and flight summary

All flights originated from the Nashville International Airport (BNA) and covered an approximately 80 x 100 km^2 area roughly centered over the Nashville metropolitan area with a series of 14 parallel fight lines each offset across track from the previous line by 8 km. The C130 was flown at a constant altitude of 6.1 km above mean sea level at a air speed of about 400 km/hr. The flight path for July 11, typical of the pattern flown on the other three days is shown in Fig. 2. overlaid on a map of the region. Each flight day the pattern was oriented so that the flight lines ~~so that the flight lines~~ were perpendicular to the predicted surface winds in an attempt to intercept any plumes, either from the several power plants in the area or from the central urban area, on multiple lines. Unfortunately, the near surface winds were very light and variable and often changed direction during the flight. Radiometric calibrations were performed at the turnaround between lines. Typically the flights started in the late morning after breakup of the nocturnal inversion and lasted about 4.5 hr. Data collection times and orientation of the flight pattern for the four flights are listed in Table 1. All scenes were observed using a step and stare approach, where a spot on the ground was observed for ~30 s, allowing the accumulation of ~10 spectral scans in each of the four spectral bands. At the end of 30 s, the instrument pointing mirror was advanced to and locked onto the next scene. This approach eliminates the introduction of

Table 1. Data Collection Local Times. Times are Central Daylight Time (CDT)

Date 1995	Start Time CDT	End Time CDT	Duration Hours	Flt. Pattern orientation*	Scenes Analyzed
7/7	11:48	15:55	4:07	110	253
7/11	10:30	14:34	4:04	180	229
7/12	10:10	14:20	4:10	180	260
7/13	13:49	17:48	4:59	135	249

* Compass direction in degrees for a line perpendicular to flight fight lines

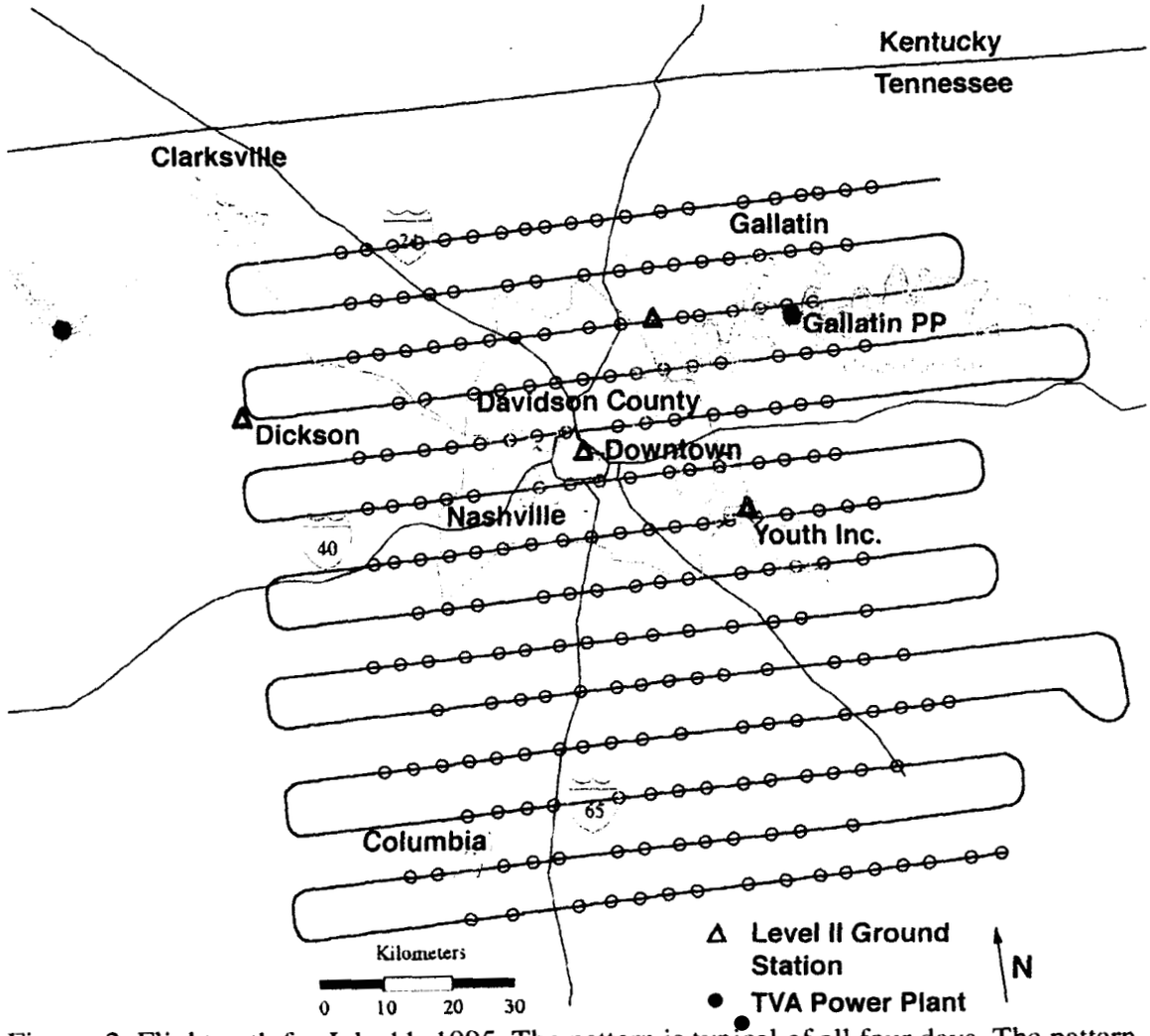

Figure. 2. Flight path for July 11, 1995. The pattern is typical of all four days. The pattern was rotated so that flight lines were perpendicular to predicted surface winds. The AES measurement locations are indicated by open circles.

noise caused by the spatial variation in radiance over a scene. The locations of the observed scenes for the July 11 flight are indicated in Fig. 2 by open circles. About 250 scenes were observed on each flight. The number of scenes used in the analysis of each day is included in Table 1.

2.3 Ancillary Data Sets

Several data sets collected as part of the SOS summer campaign aided in the processing and analysis of the AES data. Sonde profiles of temperature, relative humidity, and ozone were used as an *a priori* estimate of atmospheric state and as rough check of the retrieved

radiance noise in the measurement, helping to confirming this assertion. O_3 line parameter errors are estimated to have less than a 2% effect on the retrieved amount of O_3 based on recent work of *Rinsland et al* [1996]. They have compared high resolution IR spectrometer measurements of O_3 column amounts with those measured simultaneously with a Dobson spectrophotometer. In the 1127-1168 cm^{-1} region of the ν_1 band of O_3 they find the infrared measured O_3 total column amounts to be systematically low by ~2%. While these measurements were heavily weighted in the stratosphere in a slightly higher wavenumber region of the ν_1 ozone band than the AES retrieval, we take this as an upper limit for errors caused by line parameter errors in the AES O_3 column amounts.

Water is somewhat more problematic. Although improvements in H_2O line parameter and in continuum estimates is an active area of research [*L. Strow et al.* 1998; *D. C. Tobin et al.*, 1996], we are unaware of an any detailed study of the quantitative effects of H_2O line parameters errors on the line-by-line based infrared retrievals using the 1000-1300 cm^{-1} spectral region. Residuals between the measured AES spectra and the best retrieval calculated spectra suggest some systematic errors in H_2O line parameters. Fig. 3 shows a typical AES spectrum in the 1000-1100 cm^{-1} range where differences between the measured and calculated spectrum are noted. With the exception of water lines, residuals for lines of all other species represented in this region are consistent with the noise of the measurement. To estimate retrieval errors due to errors in H_2O line parameters, we compare the retrievals carried out using just the HITRAN96 line list to ones that include Toth's improved H_2O line parameters. The inclusion of Toth's parameters increases column H_2O by about 3% while reducing residuals by about 50% in the 950-1150 cm-1 spectral range. Assuming the remaining difference between the residuals and the estimated statistical noise is due to H_2O

Table 3 Retrieved parameter error estimates and smoothing information

Parameter	Measurement Error		Model Parameter Error		Line Parameter Errors	Fraction of Explained Variance
	statistical (1 σ)	systematic	error from fixed H_2O	error from fixed T		
T (0-1 km)	±1.33 K	±1.18 K	±1.0 K		---	0.90
H_2O (0-5.9 km)	±0.8 %	±1.3 %		±3.8 %	±6 %	0.95
O_3 (0-5.9 km)	±4.6 %	±4.2 %		±2.6 %	±2 %	0.97
CO (0-5.9 km)	±4.7 %	±3.6 %		±3.5 %	---	0.97

results. Ozone sondes were released once a day near noon local time at SOS sites near Hendersonville, TN (20 km north northeast of Nashville) or the dam on the Old Hickory Reservoir (23 km northeast of Nashville). The Hendersonville data were collected by the Georgia Institute of Technology, School of Earth and Atmospheric Sciences, and the Old Hickory data by the NOAA Climate Monitoring and Diagnostics Laboratory. Twice daily weather sondes released by the National Weather Service at the Nashville International Airport (BNA) were also employed. SOS also supported several ground monitoring stations that collected detailed chemical and meteorological data throughout the summer. Ozone and meteorological data collected at these stations, called Level II stations and indicated on the map in Fig 2, are referred to in the discussions.

2.3 Data Processing

The instrument records interferograms that are transformed to radiometrically calibrated spectral radiances from which atmospheric state parameters are retrieved using an iterative weighted least squares inversion. A prime factor Fast Fourier Transform [*Oppenheim and Schafer*, 1975] together with the *Forman et al* [1966] phase correction technique are used to transform the double sided interferograms into spectra. Individual spectra are calibrated with a simple linear relationship using coefficients derived inflight observations of the radiometric calibration source at temperatures of 290 K and 350 K. Cloud contaminated spectra are discarded using the video record of the scene and a minimum radiance criterion. Cloud free spectra (typically 16-30) of a scene are then averaged over pixels and scans to arrive at the spectra used in the atmospheric retrieval.

The retrieval process, the method by which atmospheric parameters are derived from the spectrum of a scene, uses the Sequential Estimation Algorithm for Simultaneous and Concurrent Retrieval of Atmospheric Parameter Estimates (SEASCRAPE) developed at JPL [*Sparks,* 1997; *Sparks et al.*, 1996]. SEASCRAPE consists of a line-by-line atmospheric radiative transfer model that generates synthetic spectra and an inversion algorithm that estimates atmospheric parameters and their uncertainties. The HITRAN96 spectral database [*Rothman et al.*, 1998, *Rothman et al.*, 1992] is the primary source of line parameters. The line parameters for several bands of H_2O were updated with the most recent results of *Toth* (unpublished data, 1997) and the H2O "continuum" was calculated using *Clough's* [1995] model. The inversion algorithm uses a sequential parameter estimation method known as the square root information filter [*Bierman*, 1977] to implement the optimal estimation approach to retrievals described by *Rodgers* [1976,

1990]. An advantage of this retrieval approach is that it provides an objective estimate of the atmospheric parameters and a formal analysis of their uncertainties.

The retrievals were carried out in two consecutive steps. In the first step, atmospheric temperature alone was retrieved from the 750 - 775 cm^{-1} spectral range, a region dominated by CO_2 lines. The ozone sonde measurements of H_2O were used to estimate the water profile and 365 ppmv was assumed for the abundance of CO_2. The resulting temperature profile was used in the second step for simultaneous retrieval of H_2O, O_3 and CO using 750 - 900 cm^{-1}, 950 - 1350 cm^{-1} and 1950 - 2200 cm^{-1} spectral ranges. Attempts to retrieve temperature and species simultaneously with the entire recorded spectral range gave unphysical temperature profiles. Inspection of the radiance partial derivatives with respect to temperature shows that a large fraction of the temperature information comes from H_2O lines. The improvement we attained by limiting the temperature retrieval to the 750 - 775 cm^{-1} spectral region which is dominated by CO_2 and few H_2O lines, suggest that the accuracy of the temperature dependence of water lines and water continuum over the 750 - 2200 cm^{-1} may be insufficient to permit a simultaneous retrieval of temperature and H_2O.

All retrievals are started with the daily ozone sonde profiles of temperature, humidity, and O_3 as an initial estimate ("first guess") of the atmospheric state. The ozone sonde profiles also served as an *a priori* definition of the state of the atmosphere. The role of the *a priori* is to add numerical stability to the retrieval process; however, it must be properly weighted, to avoid over-constraining the retrieved parameters. The relative contributions of the *a priori* to and the measurements is discussed below in the error analysis section. Surface emission is the largest contribution to all measured radiances and is accounted for by the retrieval of surface brightness. Nitrous oxide and CH_4 were also included in the retrieval but are not reported here. The amount of N_2O was highly constrained at 315 ppbv since its abundance expected to be constant over the observed 0-6 km altitude range. The retrieved values for CH_4 are about 20% greater than would be predicted from climatological data. We do not believe the retrieved CH_4 accurately reflects the true amount of CH_4 in the Middle Tennessee region. The 1250-1350 cm^{-1} spectral region used to retrieve CH_4 is dominated by water absorption and we believe the high retrieved values are an artifact of slightly mismodeled H_2O opacities in this spectral region.

Although we report column average volume mixing ratios, the radiative transfer is calculated on a vertical grid with spacing between 100 m and 1000 m, depending on altitude. Ozone and H_2O were retrieved on a vertical grid with 3 and 4 vertical layers

respectively. Since retrieved values of these two species for adjacent layers are corrolated, consistent with the expected vertical resolution (~3.5 km for O_3 and ~1.5 km for H_20), total column values computed from the layer amounts are reported. Temperature was retrieved on a 1 km grid, but was constrained with an 8 km correlation distance. This distance, derived from sonde temperature profiles collected during the Nashville deployment, maintains the numerical stability of the temperature retrieval, while allowing enough freedom to arrive at meaningful profiles. Here we report the temperature for the lowest 1 km since it is most easily compared to ground measurements.

The retrieved quantities were binned and averaged by geographic location to improve signal-to-noise and to present the data on a spatial scale representative of the geographic spacing of the individual measurements. The grid of 16 km x 16 km bins was chosen to encompass two flight lines.

2.4 Measurement and Retrieval Errors

Uncertainties in the retrieved quantities result both from measurement and retrieval errors. The terminology and the approach for analyzing error sources follows that of *Rodgers* [1990]. Measurement errors are defined as the uncertainties in the retrieved parameters due to statistical (noise) and systematic errors in the measured radiances. Noise is estimated directly from the measured spectra. Systematic errors in the measured radiances result mainly from uncertainties in the calibration. The major sources are uncertainties in the emissivity of the onboard calibration source, in the knowledge of the surrounding radiometric environment, and in corrections for the transmission of the window in the bottom of the plane through which the measurements are made. The noise equivalent radiance for the statistical and systematic measurements errors for a single spectral point is summarized in Table 2.

Many spectral points contribute information to the retrieval of each atmospheric parameter. The statistical errors in the retrieved parameters are determined directly from the retrieval process which uses the noise estimate together with the dependence of the radiance on a parameter's value (i.e. the Jacobian matrix) to estimate the noise in a retrieved parameter. The effects of the systematic errors were estimated by adding errors to the measured radiances and performing a retrieval to find consequent parameter variation. The estimates for these two types of errors are listed in Table 3.

Table 2. Summary of spectral measurement errors for a single spectral point. The propagation of these errors into the retrieved quantities is ~~are~~ listed in Table 3.

Filter name	2B1	1B1	1B2	1A1
Frequency range	750-900 cm^{-1}	950-1150 cm^{-1}	1150-1350 cm^{-1}	1950-2200 cm^{-1}
Noise Equivalent Radiance $\mu W sr^{-1} cm^{-2} (cm^{-1})^{-1}$	± 0.30	± 0.084	± 0.066	± 0.033
Calibration Radiance Errors $\mu W sr^{-1} cm^{-2} (cm^{-1})^{-1}$	± 0.19	± 0.14	± 0.10	± 0.15

Model parameters errors are caused by applied constraints and by inaccuracies in the parameters used to define atmospheric state. The main source of this type of error in the retrievals reported here arises from the two-step process where species profiles are fixed for the retrieval of temperature and the resulting temperature profile fixed for the retrieval of species abundances. (In an unbiased retrieval all state parameters would be retrieved simultaneously.) The potential error resulting from these constraints ~~were~~ estimated by perturbing the fixed profile, either H_2O or temperature, and noting changes in the retrieved parameters. In the retrieval of temperature the water vapor profile was perturbed by ±20% between the surface and 1 km, the largest variation seen in the sonde data during the 10 day deployment period. The potential error in the species retrieval resulting from the fixed temperature profile was investigated by perturbing the temperature profile by ±2 K. The resulting uncertainties are summarized in Table 3. A second possible parameter type error results from the use of a constant CO_2 abundance. This was investigated by perturbing the CO_2 abundance by ±20 ppm which caused a ±0.26 K change in retrieved temperature.

Approximations in the radiative transfer calculation and inadequacies in the spectral line parameters introduce what are referred to as forward model errors. The physics, algorithms, and mechanics of the SEASCRAPE forward model have been verified through extensive intercomparisons with other established forward models such as GENLN2 [*Edwards*, 1988, 1992] and LBLRTM [*Clough et al.*, 1995] demonstrating that these factors have a negligible impact on retrieval errors. Errors introduced by spectral line parameters (line position, line shape, pressure broadening parameters, etc.) are difficult to quantify. The line parameters for CO_2, CO, and N_2O for the spectral regions used here are generally known with sufficient accuracy to have a negligible effect on the retrieval errors. The residuals (forward model spectra - measured spectra) for these species are equal to the

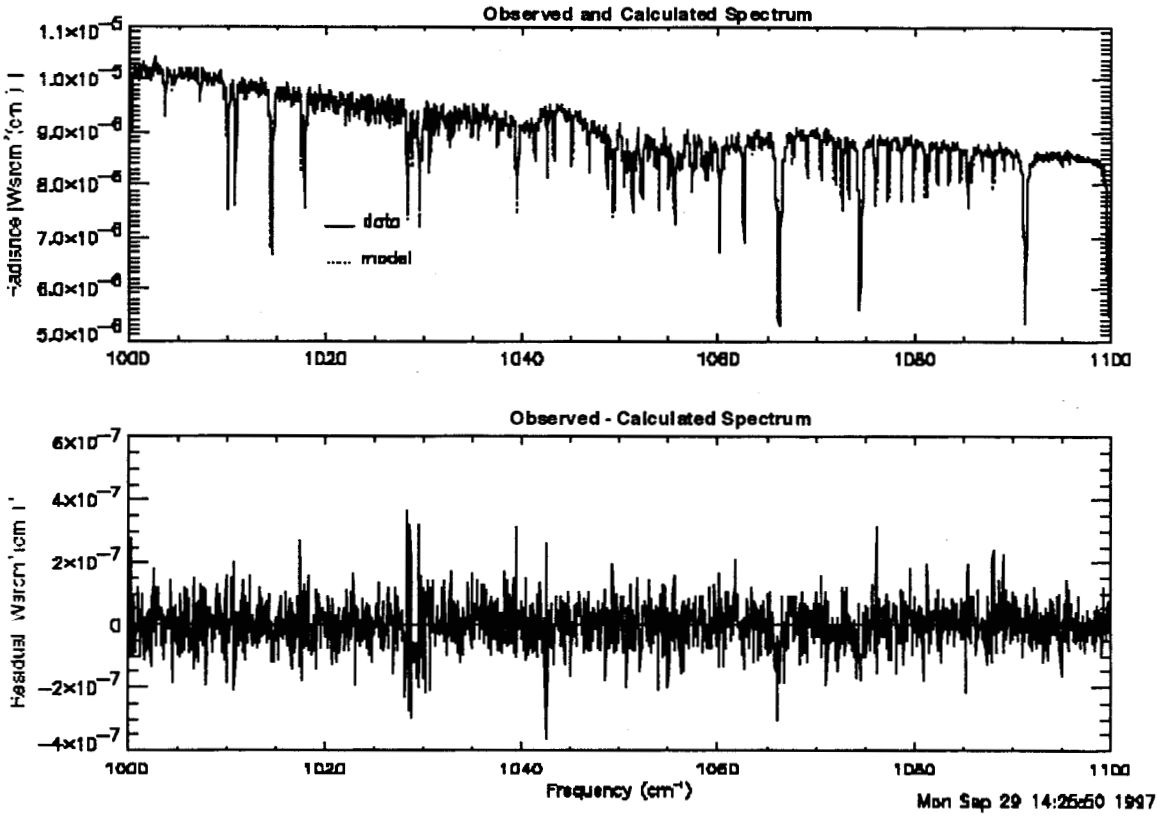

Figure 3. Typical AES spectrum and computed spectrum for the 1000-1100 cm-1 spectral range. Bottom panel is the difference between the measured and the computed spectrum.

line parameter inaccuracies in the HITRAN96 line list and not accounted for with Toth's corrections, we estimate H_2O column errors of about 6% due to H_2O line parameter errors.

Depending on the signal-to-noise of the data and details of the retrieval setup, the *a priori* can contribute to the retrieved results. The fraction of explained variance [*Clough et al.* 1995] quantitatively relates the fraction the *a priori* contributes to the retrieved value. A value of one means that all the information used to retrieve a parameter was obtained from the measured radiance while a value of zero means that the retrieved parameter is the *a priori*. value. The fraction of explained variances for the AES retrievals are listed in Table 3.

3 Results and Discussion

3.1 Overview of geography and weather

The city of Nashville and the surrounding Davidson county metropolitan area has a population of just over half a million. The urban area is surrounded by mixed forest and farm lands. This relative isolation from other urban areas combined with the area's inability to meet federal ozone standards provided much of the motivation for choosing the Nashville/Davidson area as a focus of the 1995 SOS campaign. Several coal burning power plants in the region surrounding Nashville also provide an opportunity to observe the photochemical evolution of plumes and their interaction with the urban and rural emissions.

The area around Nashville is generally flat with some rolling terrain. The surface heights range from 120 m to 360 m above sea level over the region studied. We estimate that the urban area occupies only 3-4% of the area covered on a flight so that the vast majority of the observations were taken over rural, sparsely populated areas.

An overview of the weather during the 1995 SOS campaign has been given by *NcNider* [1998]. Here, we provide a brief description of the conditions during the period of the AES data collection. On the evening of July 6, a surface cold front passed through the Nashville area leaving behind a relatively stable dry atmosphere and marking the beginning of a warming trend and the development of hot, dry and nearly stagnant conditions that persisted throughout the duration of the AES measurement period. The conditions in the region were dominated by a strong high pressure ridge that slowly moved from the southeast Midwest, across Kentucky, and eastward to the mid-Atlantic eastern seaboard during the measurement period. Daily high temperatures were generally quite high, 28-34 C, with very light surface winds. There was a gradual increase in afternoon haziness and cumulus clouds throughout the period. Table 4 lists AES flight averages and standard deviations of temperature (0-1 km), H_2O, O_3, and CO. The trends in the averages for temperature and water vapor follow those of the ground stations. The most notable difference between ground measurements and the AES results are the high values of O_3 and CO on July 7. This is discussed further below. The standard deviations of the flight averaged temperature are near the estimates of statistical error (1.3 K) for this parameter,

Table 4. Flight averages and standard deviations of retrieved quantities.

Date 1995	T (0-1 km) K	σ_T K	H_2O ppmv	σ_{H2O} ppmv	O_3 ppbv	σ_{O3} ppbv	CO ppbv	σ_{CO} ppbv
7/7	296.0	1.4	632	40	71	6	110	16
7/11	296.6	1.1	983	49	63	5	92	13
7/12	299.0	1.2	1069	63	64	4	96	14
7/13	301.0	1.6	1196	74	68	6	109	15

suggesting that temperature variability over the area is relatively small. The standard deviations of H_2O, O_3 and CO are approximately factors of 8, 2 and 3 greater respectively than the estimated statistical errors of a single measurement.

3.2 Time variability

The data collection strategy mixes time and spatial variability leaving the possibility that the at least some variations in ozone concentrations observed in the AES data are the result of daily cycle of nightly deposition followed by photochemically driven formation during the day. The flights on July 11 and July 12 were during periods when ozone levels on the ground were increasing from the normal night time lows toward afternoon maxima, while on July 13 O_3 levels on the ground were nearly constant during the afternoon flight. Figure 4 shows the flight line (E-W or W-E transit in Fig 2) averages of temperature and ozone as a function of time for the AES flights. On July 7 the variation in ozone shown in Fig. 4 is

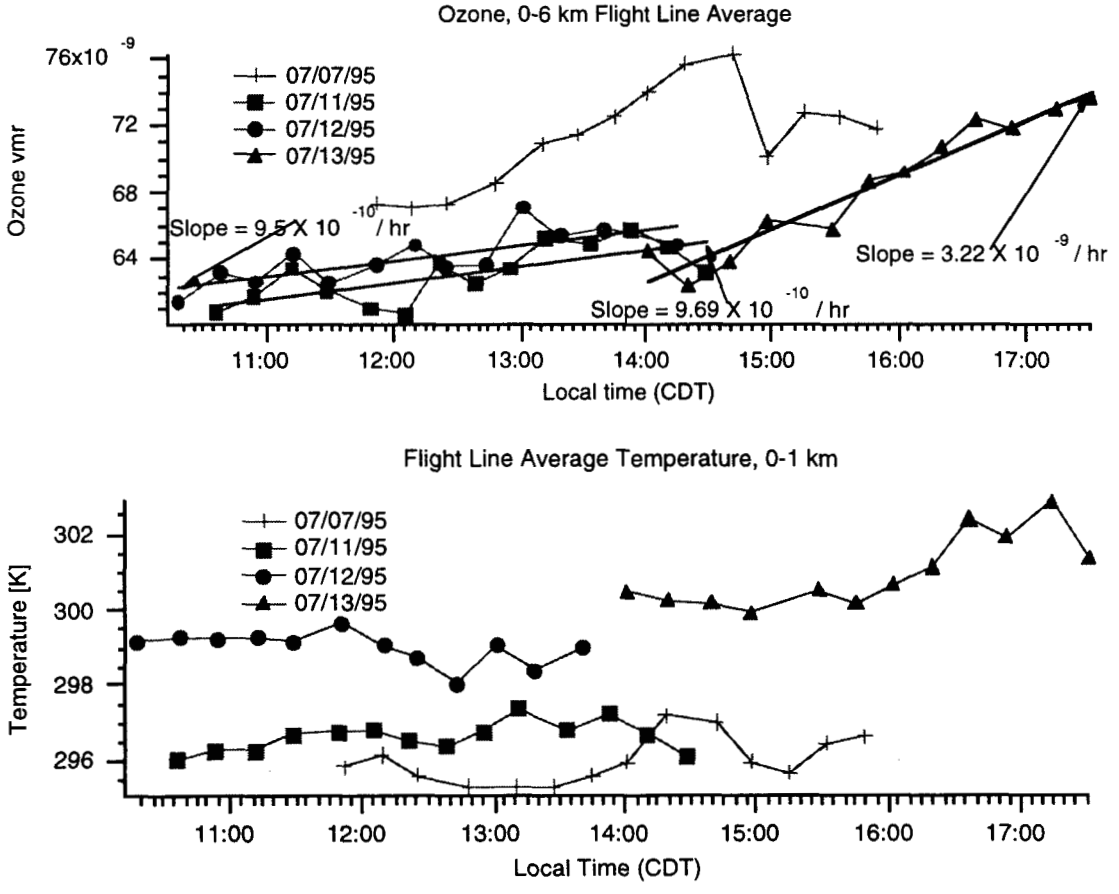

Figure 4. Flight line averages of O_3 (top) and temperature (bottom) as a function of time of measurement.

inconsistent with the spatial and temporal variations observed by ground stations in the region. This is discussed in more detail in Section 3.3. The latter three days show nearly linear increases of O_3 with time. The slope of the straight line fit through the data on the July 11 and July 12 are consistent with the daytime changes observed at ground stations. On July 13 surface station ozone levels were nearly constant during the data collection period, suggesting that the trend in ozone observed with AES on this day reflects a spatial gradient. The time variations in temperature are small, all less than 3 K over a flight period, and show no easily interpreted time trend.

If it is assumed that the linear trends in O_3 observed on July 11, 12 and 13 are only a function of time the trend is easily removed from the data. While this adjustment reduces the differences between the minima and maxima of the mapped data described in Section 3, there is little qualitative change to the structure shown in the maps.

3.3 Mapped Retrieved Quantities

The mapped retrieved quantities for the four days are shown in Figs. 5-8. The reader should be reminded that the binned data are means of ~6 individual measurements so that the statistical errors are reduced by ~2.4 compared to those listed in Table 3. While the maps of temperature and H_2O contain statistically significant variations, it is difficult to relate the details to either the weather or topography. A mesoscale assimilation model of the weather is probably required to shed light on the observed features. They are included here to document the conditions under which O_3 and CO are observed. In contrast the maps of O_3 and CO contain several features that can be immediately related to the chemistry and dynamics of the region.

3.3.1 July 7

July 7 stands out from the other three days in both the meteorology and the levels of O_3 and CO observed by AES. This day followed the passage of a cold front late the previous afternoon leaving a relatively dry upper troposphere (dew point less than -20 C above 3 km from the BNA sonde) and clean near surface atmosphere. The BNA soundings show the winds were out of the west to northwest and became more northwesterly by the evening at

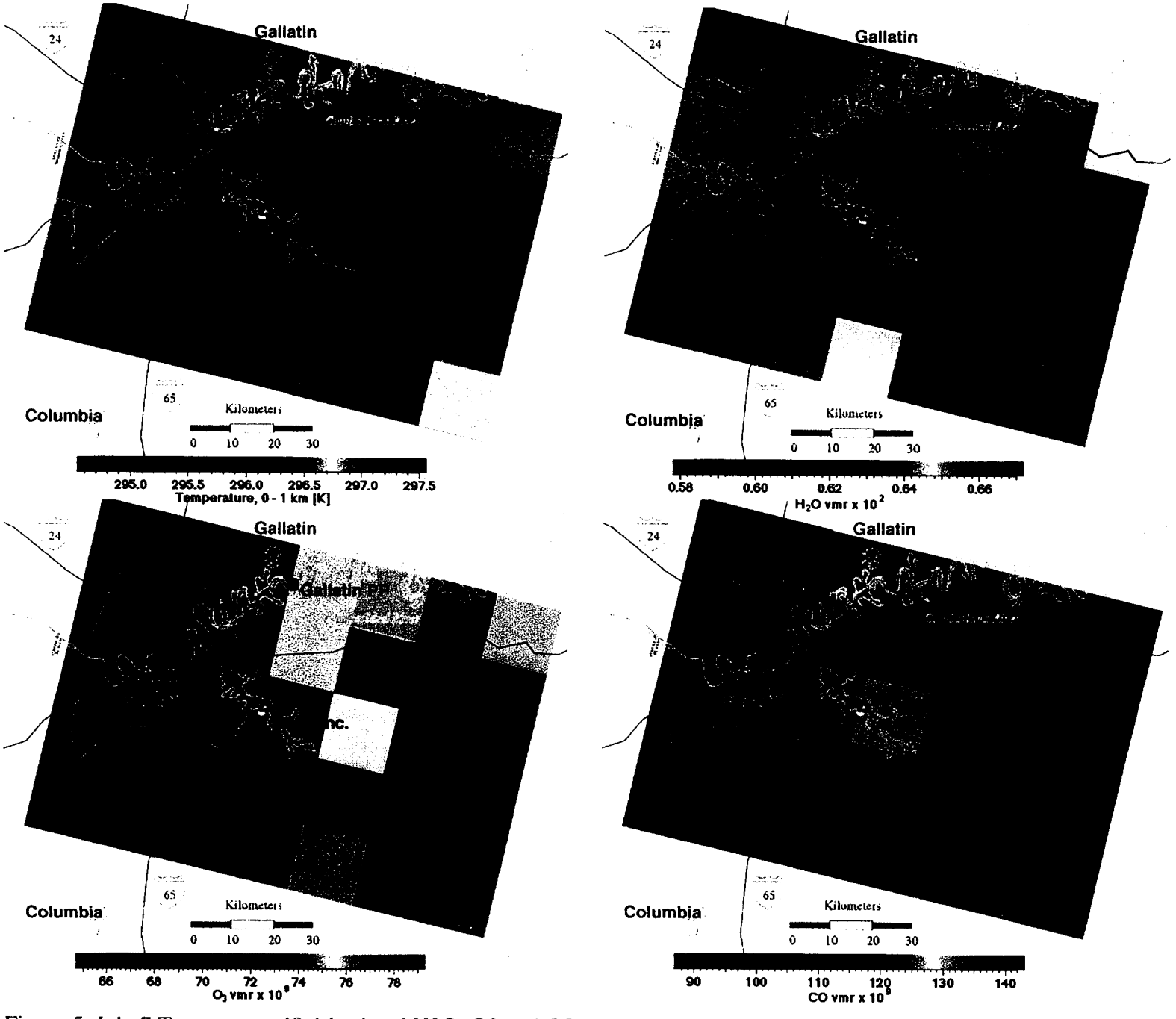

Figure 5. July 7 Temperature [0-1 km] and H2O, O3 and CO, 0-6 km column average vmr.

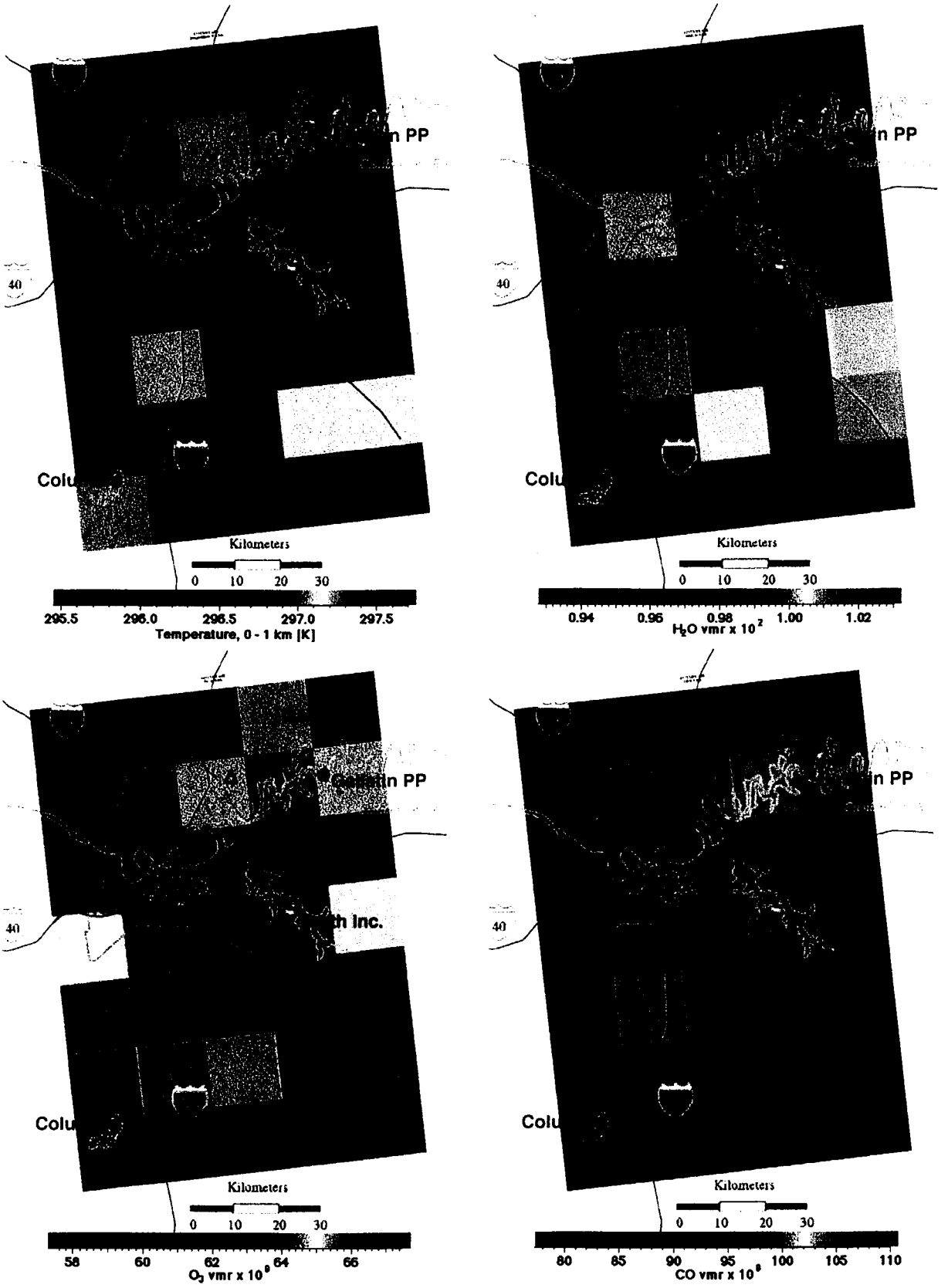

Figure 6. July 11 Temperature [0-1 km] and H2O, O3 and CO, 0-6 km column average vmr.

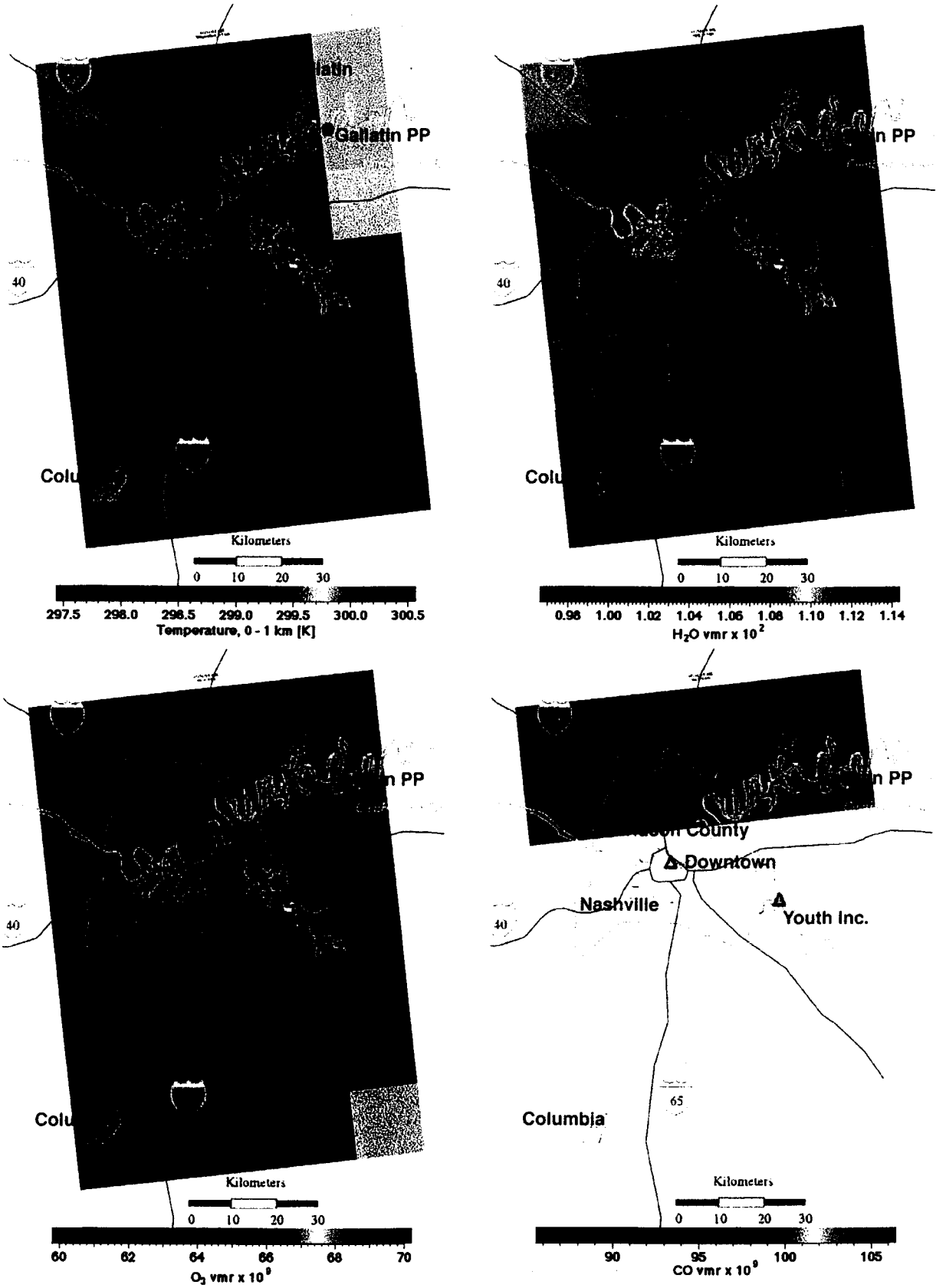

Figure 7. July 12 Temperature [0-1 km] and H2O, O3 and CO, 0-6 km column average vmr.

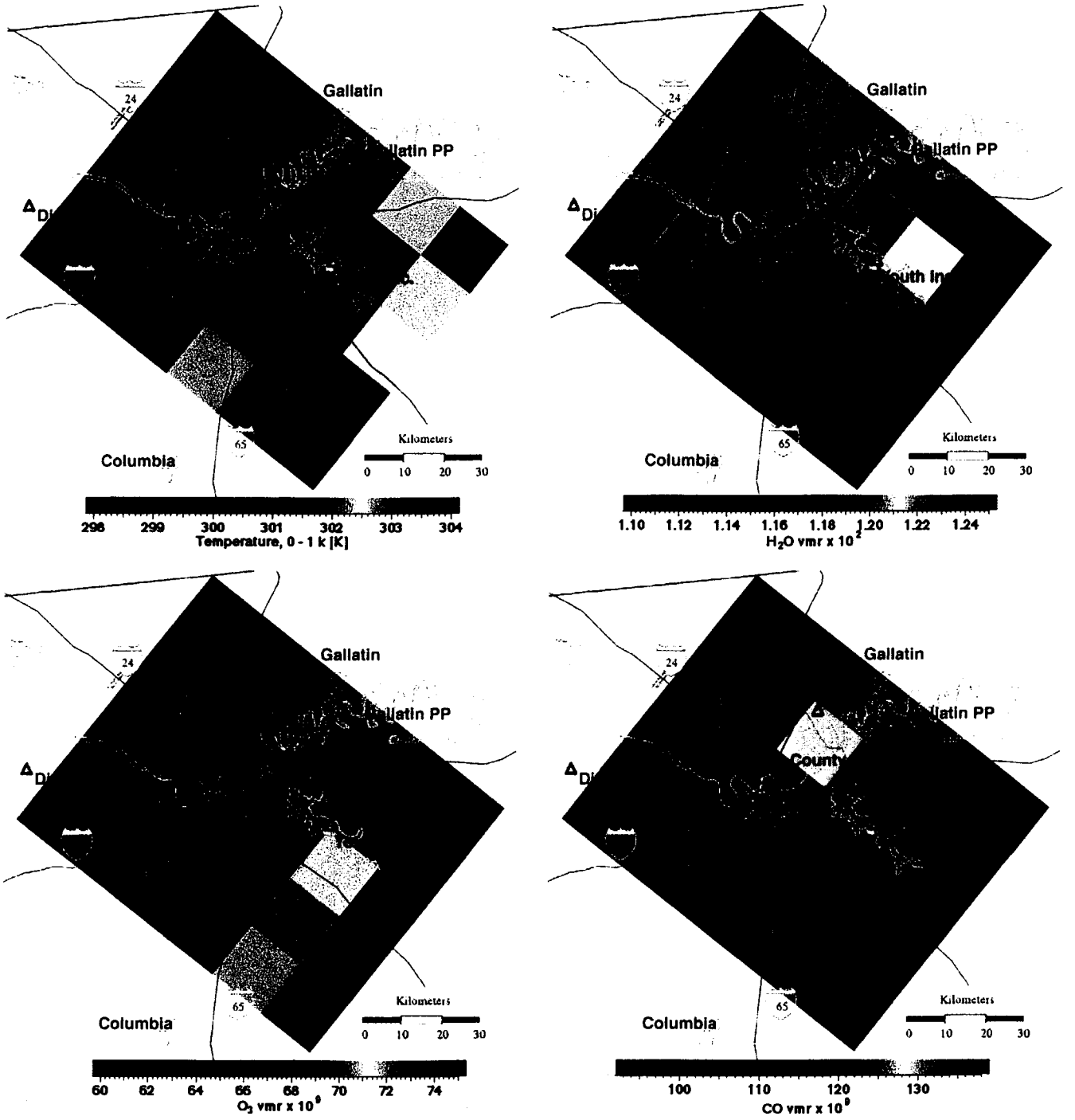

Figure 8. July 13 Temperature [0-1 km] and H2O, O3 and CO, 0-6 km column average vmr.

5 to 15 m/s throughout the 0-6 km altitude range. Of the four days, the Downtown Level II monitoring station recorded the lowest ozone afternoon maximum (68 ppbv at 16:00), and with an afternoon maximum temperature of 28.2 C this was also the coolest of the four days.

The AES measurements also show this to be the coolest and driest of the four days but the O_3 and CO levels observed by AES and averaged over the measurement area are the highest of the four days (although 7/13 is a very close second.) This day also has more coherent structure than the other three days, particularly in the O_3 and CO fields. There is a readily distinguishable region of high O_3 and CO extending from the middle of the northern edge of the mapped area to the south and southeast.

The high values of CO in the vicinity of the Gallatin coal burning power plant might suggest that the plant was releasing copious amounts of CO. However, economics of power plant operations demand high combustion efficiencies, thus minimizing CO emissions. In addition, records for power plants in the study region show no unusual operating conditions on this day (*J. Meagher*, private communication.) further arguing against a power plant as the source of the observed high concentrations of CO.

The ozone sonde released at the New Hendersonville site at noon suggests an explanation. The sonde shows a region of enhanced ozone (~95 ppbv against a background of 60 ppb) between 2.8 and 4.6 km altitude with three somewhat resolved layers, and a fourth, less concentrated layer between 5.2 and 6 km altitude. The AES data in combination with the ground measurements and ozone sonde strongly suggest that the high concentrations of O_3 and CO are well above the surface.

Layers of elevated ozone in the free troposphere have been observed by many investigators [*Kleinman, L. I. et al.*, 1996; *Trainer et al.*, 1995;]. It has been suggested that that vertical transport of near surface polluted air mass by both synoptic scale vertical motions [*Fast, J. D. and C. M. Berkowitz*, 1996] and boundary layer convective events [*Pickering, K. E. et al.*, 1992; and *Elliot, S. et al.*, 1996] may account for the development of such enhanced O_3 regions in the free troposphere. The downward transport of ozone rich air from the stratosphere has also been proposed as a mechanism for enhanced tropospheric O_3 in some cases [*Oltmans, S. J. et al.*, 1996].

The region of high abundance of both CO and O_3 strongly argues for an anthropogenic source for the elevated region. The lack of a credible nearby source for the elevated CO and O_3, combined with the passage of the front through the region the previous afternoon suggest that vertical transport of polluted air at a distant source followed by transport into the Nashville area would explain the regions of high O_3 and CO observed by AES. The upper tropospheric (3 - 6 km) winds derived from the BNA soundings indicate a source to the north to northwest.

3.3.2 July 11, 12 and 13

The conditions during this three day period were stagnant with light (less than 2 m/s), highly variable winds near the surface, and afternoon temperatures near 35 C. For the 12 hrs. prior to the flights the surface winds on July 11 were predominately out of the north to northwest and on July 12 and 13 they were predominately out of the southeast. Above the boundary layer, winds were out of the north to north-east at 5-8 m/s on July 11 and 12 but became more easterly on July 13 at 5-12 m/s as a high pressure ridge over Kentucky moved to the northeast. The three days represent a view of the evolution of the stagnant conditions and are treated together.

The Downtown ground stations showed the highest ozone values on July 12 (140 ppb at 14:30 CDT) while the Youth station, located about 28 km south-east of the Downtown measured the highest levels on July 11 (110 ppb at 17:30 CDT). Zero to 5.9 km column average O3 concentrations derived from the ozone sondes were lowest on July 12 (57.6 ppbv) and highest on July 13 (84.0 ppbv), although the July 11 column amount (59.1 ppbv) was very close to that of July 12. The AES measurements differ somewhat from the ground station measurements and the ozone sondes. Over the three day period, the flight averaged values of all four atmospheric variables measured by AES increased (c.f. Table 4). We attribute the differences between the surface, the sondes and the AES measurements to spatial variability over the region, an assertion that is supported by the spatial variability seen in the mapped data.

The AES measurements have several common features that persist over the three day period. Ozone levels are highest to the south and south east of the city center, showing some evidence for an urban plume, especially on July 11 and 12. On July 11 there is a large region of high ozone extending south to southwest of the urban area and on July 12 a region extending from the urban area to the southwest. On July 13 higher levels of O_3 are

found across a broad area southeast of the urban area. (Note also higher temperature and lower water vapor in this region on July 13) There is a region of enhanced O_3 extending from the area around the Gallatin power plant southward that would appear to indicative of a plume from the Gallatin power plant. However, this interpretation is inconsistent with both the surface and BNA sonde winds below 2 km altitude. On all three days the highest ozone levels are observed a considerable distance from the city center. On July 11 the maximum is at 30 km south west of the city center, on July 12 it is at 40 km south of the city center. On July 13 at about 50 km south and east of the city center. This is in contrast to surface measurements over the region which show highest ozone levels near the city center, however surface measurements are very sparse in the areas of highest ozone detected with AES.

Regions of high CO are somewhat better defined than those for O_3 and are near the city center. On July 11 a region to the southwest shows the highest levels, while on July 13 the highest levels are found to the northwest to north of the city. Unfortunately, an instrument malfunction on July 12 precluded CO measurements over the entire flight. The locations of highest concentrations are consistent with advection from the urban center by surface winds.

On July 11 the spatial distribution of both CO and O_3 are generally consistent with a weak northerly to northeasterly surface flow, with the Nashville urban area as the primary source of CO and O_3 precursors. However, the high levels of O_3 to south on July 12 and to the southeast on July 13 would suggest that something other than simple transport at the surface is controlling the column distribution in the mapped area. High levels of O_3 above 3 km would imply advection from a considerable distance since winds above this altitude were relatively steady and with speeds greater than 5 m/s (typically greater than 10 m/s) throughout the three day period. The O_3 sondes on July 11 and 13 indicate the existence of layers of enhanced O_3 at 0.7-1.2 km (July 11) and at 1.8-2.2 km (July 13) just above the afternoon boundary layer. Layers of O_3 well above the surface contribute to the AES column measurements, and spatial variability of such layers would be consistent with the AES observations. Winds were also light and variable in the 1-2 km range during this three day period based on wind profiles recorded at the Dickson Level II site. Vertical transport to this region through convection driven by the strong daily insolation over the three day period as evidenced by the development of cumulus clouds each afternoon is a mechanism that might allow for a more local source of parcels of polluted air that could lead to the

higher O_3 levels above the boundary layer. More detailed information on the vertical distribution of O_3 and its precursors is probably required to elucidate a mechanism.

4. Conclusions

While surface and near surface measurements are a vital element to unraveling the factors that control the formation and distribution of tropospheric ozone the results presented here suggest that in some conditions the highest concentrations of O_3 may be well above the surface. Several theoretical [*Jacob et al.*, 1993; *Fast and Berkowitz*, 1996] and observational studies [*Pickering et al.*, 1992; *Kleinman et al.*, 1996] have elaborated on the importance of transport in the middle troposphere to the regional and global distribution of ozone. The observations of July 7, provide more evidence that middle tropospheric transport is an important factor in determining regional distributions of O_3 and its precursors.

The results for July 11-13 illustrate the difficulty of determining the distribution of tropospheric ozone from surface measurements alone and the utility of broad, dense spatial coverage. The areas where the highest column levels of O_3 are observed are relatively distant from the urban center where surface measurements are often concentrated. This is not to say that surface ozone levels in regions predominated by urban emissions are likely to be highest in regions distant from the urban area, but that in the troposphere as a whole the highest levels may be found at some distance from the urban center. A more complete analysis accounting for local meteorology, distributions of ozone precursors such as NO_x and volatile organic hydrocarbons over the entire region and altitude range is probably required to unravel the mechanisms that determine the spatial distributions observed by AES. Many of the essential elements needed for a more complete analysis were collected during the SOS 1995 campaign and future collaborative efforts have the potential to greatly enhance the understanding of all the observations made during the campaign.

Previous flights of AES focused on specific target types [*Worden et al.*, 1997]. The SOS intensive campaign was the first opportunity to test the application of AES and the retrieval and analysis to tropospheric remote sensing. In this regard SOS has provided both a challenge and an ideal opportunity to improve the collection, processing and analysis of high resolution infrared remote sensing. The AES data reduction and analysis benefited greatly from the extensive collection of weather data provided through the SOS program as well as informal comparisons between our retrieved results and *in situ* measurements.

Acknowledgments.

The ozone sonde data were provided through the courtesy of J. Cordle of the Georgia Institutes of Technology and M. O'Neill of NOAA CMDL. Ground station ozone and meteorology data were provided courtesy of W. Parkhurst of the Tennessee Valley Authority Environmental Research Center. Logistical support by the Southern Oxidants Study under the direction of J. Meagher of the Tennessee Valley Authority and E. Cowlings of North Carolina State University is gratefully acknowledged. The authors thank D. Perrish and M. Trainer, C. Senff, and R. McNider for many helpful discussions. Special thanks to Flight Operations Branch of NASA/Wallops Island Flight Facility and to T. Glavich, R. Holm, C. Kurzweil and R. Steinkraus of the Jet Propulsion Laboratory without whose dedication and efforts these measurements could not have been made and to J. McNeal of NASA Headquarters for his continuing support. The research described in this paper was conducted by the Jet Propulsion Laboratory, California Institute of Technology, under a contract with the National Aeronautics and Space Administration.

References

Beer, R., *Remote Sensing by Fourier Transform Spectroscopy, Chem. Anal ., vol. 120,* edited by J. D. Winefordner, pp. 121-127, John Wiley, New York, 1992.

Beer R., and T. A. Glavich, Remote sensing of the troposphere by infrared emission spectroscopy, *Proc. SPIE Int. Soc. Opt. Eng., 1129*, 42-48, 1989.

Bierman, G. J. *Factorization methods for discrete sequential estimation, Academic Press*, New York, 1977.

Ching, J. K. S., S. T. Shipley, and E. V. Browell, Evidence for cloud venting of mixed layer ozone and aerosols, *Atmos. Environ.*, *22*, 225-242, 1988.

Clarke, J. F., and J. K. S. Ching, Aircraft observations of regional transport of ozone in the northeastern United States, *Atmos. Environ.*, *17*, 1703-1712, 1983.

Clough, S. A. The water vapor continuum and its role in remote sensing. In *Optical Remote Sensing of the Atmosphere, 2*, 76-78, OSA Tech. Digest Services, Washington D. C., February 1995.

Clough, S. A., C. P. Rinsland and P. D. Brown, Retrieval of tropospheric ozone from simulations of nadir spectral radiances as observed from space, *J. Geophys. Res.*, *100*, 16,579-16,593, 1995.

Edwards, D. P. GENLN2: A general line-by-line atmospheric transmittance and radiance model. Version 3 description and users guide, NCAR Report TN-367+STR, Natl. Cent. for Atmos. Res., Boulder, CO, 1992

Edwards, D. P., GENLN2: Atmospheric transmittance and radiance calculations using line-by-line computer models, in Modeling of the Atmosphere, L. S. Rothman, ed., *Proc. Soc. Photo-Opt. Instrum. Eng., 292*, 94-116, 1988.

Elliot, S., C. J. Kao, F. Gifford, S. Barr, M. Shen, R. P. Turco and M. Jacobson, *Atmos. Enviro. 30*, 4263-4274, 1996.

Fast, D. J. and C. M. Berkowitz, A modeling study of boundary layer processes associated with ozone layers observed during the 1993 North Atlantic Regional Experiment, *J. Geophys. Res.*, *101*, 28,683-28,699, 1996.

Foreman, M., W. H. Steel and G. A. Vanassee, Correction of asymetric interferograms obtained in Fourier spectroscopy, *J. Opt. Soc. Am., 56*, 59, 1960.

Hübler, G., P. Alveraz, P. Daum, R. Denis, N. Gillani, L. Kleinman, W. Luke, J. Meagher, D. Rider, M. Trainer, and R. Valente, An overview of the Airborne Activities during the SOS 1995 Nashville/Middle Tennessee Ozone Study, *J. Geophys. Res.*, SOS special issue.

Jacob, D. J. J. Logan, G. M. Gardner, R. M. Yevich, C. M. Spivakovsky, S. C. Wofsy, S. Sillman and M. J. Prather, Factors Regulating Ozone Over the United States and Its Export to the Global Atmosphere, *J. Geophys. Res.*, *98*, 14,817-14,826, 1993.

Kleinman, L.I., P. H. Daum, Y. Lee, S. R. Springston, L. Newman, W. R. Leaitch, C. M. Banic, G. A. Isaac and J. I. MacPherson, Measurements of O3 and related

compounds over Nova Scotia: 1. Vertical Distributions, *J. Geophys. Res.*, *101*, 29,043-29060, 1996.

Meagher, J. F., E. B. Cowling, F. C. Fehsenfeld and W. J. Parkhurst, Ozone Formation in the Southeastern United States: An Overview of the SOS Nashville/Middle Tennessee Ozone Study, *J. Geophys. Res.*, SOS special issue.

NcNider, R. T., W. B. Norris, A. J. Song, R. L. Clymer and G. Shekhar, Meteorological Conditions During the 1995 SOS Nashville/Middle Tennessee Field Intensive, *J. Geophys. Res.*, SOS special issue.

Oltmans, S. J. H. Levy II, J. M. Harris, J. T. Merril, J. L. Moody, J. A. Lathrop, E. Cuevas, M. Trainer, M. S. O'Neill, J. M Prospero, H. Vomel, and B. J. Johnson, Summer and spring ozone profiles over the North Atlantic from ozonesonde measurements, *J. Geophys. Res.*, *101*, 29,179-29,200, 1996.

Oppenheim, A. V. and R. W. Schafer, *Digital Signal Processing*, Sec. 6.4, Prentice-Hall, Englewood Cliffs, N.J., 1975.

Pickering, K. E., A. M. Thompson, J. R. Scala, W. Tao, R. R. Dickson and J. Simpson, Free tropospheric ozone production following entrainment of urban plumes into deep convection, *J. Geophys. Res.*, *97*, 17,985-18,000, 1992.

Persky, M. J., A review of spaceborne infrared Fourier transform spectrometers for remote sensing, *Rev. Sci. Instrum.*, *95*, 4763-4797, 1995.

Rinsland, C. P., B. J. Connor, N. B. Jones, I. Boyd, W. A. Matthews, A. Goldman, F. J. Murcray, D. G. Murcray, S. J. David and N. S. Pougatchev, Comparison of Infrared and Dobson total ozone columns measured from Lauder, New Zealand. *Geophys. Res. Lett, 23*, 1025-1028, 1996.

Rodgers, C. D., Retrieval of atmospheric temperature and composition from remote measurements of thermal radiation, *Rev. Geophys Space Phys., 14*, 609 - 604, 1976.

Rodgers, C. D., Characterization and error analysis of profiles retrieved from remote sounding measurements, *J. Geophys. Res.*, *95*, 5587-5595, 1990.

Rothman, L. S., et al. The HITRAN molecular database: Editions of 1991 and 1992, *J. Quant. Spectroc, Radiat. Transfer*, 48, 469-507, 1992.

Rothman, L. S., C. P. Rinsland, A. Goodman, S. T. Massie, J. M. Flaund, A. Perrin, V. Dana, J. Schoeder, A. McCann, R. R. R. Gamache, R. B. Wattson, K. Yoshino, K. Chance, K. Jucks, L. R. Brown and P. Varanasi, The HITRAN Molecular Spectroscopic Data Base and HAWKS (HITRAN Atmospheric Workstation), *J. Quant. Spectroc, Radiat. Transfer*, (in preparation) 1998.

Sparks, L., J. McComb, J. L. Fanselow, SEASCRAPE (Simultaneous and Concurrent Retrieval of Atmospheric Parameter Estimates), *NASA Tech. Brief, NPO - 19694*, 1996.

Sparks, L. Accelerated line-by-line calculation of spectral absorption coefficients to high numerical accuracy, *J. Quant. Spectrosc. Radiat. Transfer,* 57, 631-650, 1997.

Strow, L., D. C. Tobin, W. W. McMillan, S. E. Hannon, W. L. Smith, H. E. Rivercomb, and R. Kneuteson, Impact of a New Water Vapor Continuum and Line Shape Model on Observed High Resolution Infrared Radiances. *J. Quant. Spectrosc. Radiat. Transfer,* in press, 1998.

Tobin, D. C. L. L. Strow, W. J. Lafferty, and W. B. Olson. Experimental investigation of the self- and N2- broadened continuum within the v2 band of water vapor. *Appl. Opt., 35*, 1996.

Trainer, M., B. A. Ridley, B. A. Buhr, G. Kok, J. Walega, G Hübler, D. D. Parrish, and F. C. Fehsenfeld, Regional ozone and urban plumes in the southeastern United States: Birmingham, a case study, *J. Geophys. Res., 100*, 18,823-18,834, 1995.

Worden , H., R. Beer and C. P. Rinsland, Airborne infrared spectroscopy of 1994 western wildfires, *J. Geophys. Res., 102*, 1287-1299, 1997.